

# Solar H- $\alpha$ Oscillations from Intensity and Doppler Observations

Jason Jackiewicz

*New Mexico State University, Department of Astronomy, P.O. Box 30001, MSC 4500, Las Cruces, NM 88003, USA*

jasonj@nmsu.edu

K.S. Balasubramaniam

*Space Vehicles Directorate, Air Force Research Laboratory, Kirtland AFB, NM 87114, USA*

## ABSTRACT

Chromospheric wave activity around flares and filaments has been a research focus for years, and could provide indirect measurements of local conditions that are not otherwise accessible. One interesting observed phenomenon is oscillations in filaments, activated by distant flares and the large-scale waves they produce. Characteristics of these oscillations, such as periods, amplitudes, and lifetimes, can provide unique information about the filament.

We measure oscillation properties in flares and filaments from H $\alpha$  chromospheric data using a new method that provides important spatial and frequency content of the dynamics. We apply the method to two flare events where filaments are observed to oscillate and determine their properties.

We find strong oscillatory signal in flaring active regions in the chromosphere over a range of frequencies. Two filaments are found to oscillate without any detectable chromospheric wave acting as an activation mechanism. We find that filaments oscillate with periods of tens of minutes, but variations are significant at small spatial scales along the filamentary region.

The results suggest there is a frequency dependence of the oscillation amplitude, as well as a spatial dependence along single filaments that is more difficult to quantify. It also appears that the strength of the oscillations do not necessarily depend on the strength of the trigger, although there are other possible effects that make this conclusion preliminary. Applications of this technique to other events and different data sets will provide important new insights into the local energy densities and magnetic fields associated with dynamic chromospheric structures.

*Subject headings:* Sun: atmosphere - Sun: oscillations - Sun: filaments, prominences - Sun: flares - techniques: image processing

## 1. Introduction

It has been known for a long time (Ramsey & Smith 1966) that oscillations in solar prominences and filaments can be excited by distant flares. Such events have generally been characterized by so-called large- and small-amplitude oscillations according to the amplitude of their observed velocities (compared to the chromospheric sound and Alfvén velocities). Large-amplitude filament oscillations display speeds upwards of  $20 \text{ km s}^{-1}$  and periods of tens of minutes to hours, while small-amplitude oscillations typically are a few  $\text{km s}^{-1}$ , with a less well-constrained range of periods, from minutes to hours (Arregui et al. 2012). Motions are found in both transverse and longitudinal directions with respect to the filament axis.

The chromosphere displays a wealth of wave phenomena. Early detections of oscillations in  $\text{H}\alpha$  measurements were carried out by Elliott (1969), and Harvey et al. (1993) used several chromospheric lines to observe the high-frequency (5 mHz)  $p$  modes, as well as 5-min. acoustic modes, both escaping from the photosphere. However, a flare (or some other source) activating a filament oscillation is a rather rare phenomenon, quite different than the oscillations that are always present in the chromosphere. Triggers of the filament activation are thought to be Moreton waves or EUV waves produced from remote flares (Eto et al. 2002; Okamoto et al. 2004; Balasubramaniam et al. 2007, 2010; Asai et al. 2012; Li & Zhang 2012), or jets and subflares (Vršnak et al. 2007), or even erupting filaments themselves (Isobe & Tripathi 2006). It is likely that intrinsic properties of the chromosphere can be deduced from studying these oscillations, as filaments seem to have associated eigenfrequencies when excited. This could be used to probe their magnetic structure and topology more precisely than traditional observations.

Recent reviews (Tripathi et al. 2009; Arregui et al. 2012) point out that much of the detailed dynamics between the interaction of the Moreton or EUV waves with the filament, the oscillatory structure (vertical/horizontal and longitudinal/transverse), the damping mechanism, and possible causes of filament eruptions are still very open issues, as these filament oscillations have only been observed in about a dozen cases.

The scope of this work is not to directly address all the issues above, but to provide a new tool for analyzing these and similar oscillatory phenomena. We have observed two oscillating filament events, one never detected and the other previously studied by Gilbert et al. (2008). Standard analysis in previous studies typically involves reducing a three-dimensional (3D) data cube to a one-dimensional (1D) time series by spatially averaging over pixels in the filament that appear to be oscillating, and then performing a wavelet transform in time-frequency space to ascertain the variable frequency content. The reduction in dimensions has the effect of smearing possibly important spatial information. At the same time, the result may be strongly dependent on how the averaging is carried out.

Here we describe a new technique for analyzing phenomena that have dynamic spatial and temporal scales. It is an extension of a wavelet-type technique, preserving the 3D nature of the input data. Upon application, we observe properties of chromospheric oscillations that do not easily fit into the two categories described above. We observe important differences in flaring regions and regions of oscillating filaments, indicating different responses to the trigger mechanism. We also find anomalies in oscillating filaments that have and have not interacted with a strong Moreton wave. A standard analysis is also carried out for comparison.

To introduce this technique, we first describe the example data sets in § 2. We provide an overview of the algorithm in § 3, which is then applied to the data and results are shown in § 4. After comparisons of the results to standard methods and a summary are provided, discussion is given in § 5.

## 2. Data

We study two flare events observed with the United States Air Force/National Solar Observatory Improved Solar Observing Optical Network (ISOON) telescope located at Sacramento Peak, NM (Neidig et al. 1998). Full-disk solar images ( $2048 \times 2048$  pixels at  $1.1''$  sampling) at 1-minute cadence are observed in the  $6563\text{\AA}$   $\text{H}\alpha$  line center with a  $0.1\text{\AA}$  bandpass filter. Corresponding Doppler maps are also utilized, and have been constructed by the following procedure: 14 images across 14 wavelengths centered around the spectral line were gathered on a day in 2004 when there was little activity on the Sun. After calibrating the images for intensity corrections and flat-fields, spectral line profiles for each  $1.1$  arcsecond pixel were obtained, separately. From the center-of-gravity (spectral line center) for each spectral line, the intensity-difference at  $\pm 0.4\text{\AA}$ , and a Doppler shift (line-center for each pixel, mean line-center for entire image) was measured. By plotting all the points of Doppler shift versus the intensity difference, a characteristic relationship is found. For any day of observing the intensity differences, a conversion of that measure to Doppler shift is computed (assuming that the calibration holds true). In the flares and filaments considered here the  $\text{H}\alpha$  line wings remain in absorption (Balasubramaniam et al. 2004).

A solar flare of x-ray strength M8.0 occurred on May 13, 2005 around 16:13UT in active region NOAA 10759. It was a classic two-ribbon flare that also corresponded to a very large CME that delivered the most intense geomagnetic activity of 2005 (Bisi et al. 2010). Various characteristics of this well-known event have been studied (Yurchyshyn et al. 2006; Liu et al. 2007; Kazachenko et al. 2009), although this is the first time oscillations in the active region and the nearby filaments have been detected. The second event occurred on December 6, 2006, where an X-class flare erupted at about 18:40UT in NOAA 10930. For both cases,

ISOON provided high-quality intensity and Doppler data from about 4 hours before until 4 hours after flare initiation. Pre-flare snapshots of full-disk  $H\alpha$  intensity images for each data set are shown in Fig. 1. The flaring active regions (bright in  $H\alpha$ ), as well as several quiescent filaments (dark in  $H\alpha$ ) that this investigation targets are outlined in boxes.

One important difference between these two flares is that the 2006 event produced a prominent Moreton wave (Gilbert et al. 2008; Balasubramaniam et al. 2010), a fast-moving chromospheric disturbance. This particular wave propagated from the active region and interacted with several filaments on the solar disk, some quite far from the excitation location. Filament-wave interactions in this flare were studied in detail by Gilbert et al. (2008). A second important difference is the active region responsible for the 2006 event is located close to the limb, where strong (horizontal) velocity signals should be apparent in the line-of-sight Doppler observations.

### 3. Data Analysis

Studies of oscillations in filaments in the past have used velocity time series maps from both wings of a spectral line and determine when the filament transitions from red- to blueshifted, giving an estimation of the period (for example, Okamoto et al. 2004; Gilbert et al. 2008). Frequency content has also been derived by spatially averaging a set of pixels in the region of interest to produce a proxy 1D “light curve,” and then using wavelet techniques (Jain & Tripathy 1998; Maurya & Ambastha 2008; Pintér et al. 2008).

We demonstrate a simple and powerful way of visualizing these types of data, that preserves both frequency and spatio-temporal information. We generate what we call “*frequency-filtered amplitude movies*” (FFAMs), with a method similar to what would be described as 3D wavelet analysis.

To produce the FFAMs, consider a general data cube (we will be working with intensity and Doppler velocity) of 2 spatial and 1 temporal dimensions,  $f(x, y, t)$ . Assume there are  $N$  time steps (images) available. For each time step  $t_i$ , the following steps are carried out:

1. Filter the data in the time domain over a segment of length  $T$ , which in this study is always taken to be 60 minutes, thus comprising  $N_T = 60$  images. The 60-min filter tapers off quickly, but smoothly to zero at each “edge.” In other words, only the subsequent  $N_T$  images after the current time step are considered. The filtering is represented as

$$\overline{f}_i(x, y, t; T) = F_1(t; [t_i, t_i + T]) \cdot f(x, y, t), \quad (1)$$

where the brackets in the second argument of the filter  $F_1$  denote the range where it is nonzero and equal to unity. The filtered data  $\bar{f}_i$  are labeled by the particular starting time step  $i$  and the segment length  $T$ .

2. Compute the temporal power spectrum of that segment

$$P_i(x, y, \nu; T) = \left| \sum_{i=1}^{N_T} \bar{f}_i \exp(2\pi i \nu t_i) \right|^2, \quad (2)$$

where  $\nu$  is the cyclic frequency. Only the data over the segment  $T$  will contribute to the power. We subsequently convert this power spectrum to an amplitude spectrum  $A_i(x, y, \nu; T)$  to get units of velocity when using Doppler velocity data.

3. Apply a second filter  $F_2$  in frequency to the amplitude spectrum, which has a central frequency  $\nu_0$  and a bandwidth of  $\Delta\nu$ , and compute the average over the frequencies in that particular band:

$$\bar{A}_i(x, y; \nu_0, \Delta\nu, T) = \langle F_2(\nu; \nu_0 \pm \Delta\nu/2) A_i(x, y, \nu; T) \rangle_\nu, \quad (3)$$

where the  $\langle \dots \rangle_\nu$  operator indicates an average over the values of frequency in the range  $\nu_0 \pm \Delta\nu/2$ . The amplitude quantity  $\bar{A}_i$  is a two-dimensional image labeled by central frequency, bandwidth, and segment length.

4. Continue for all  $i \leq N - N_T$  (the final  $T$  minutes are not computed to avoid the “edge”). The final data product, FFAM =  $\sum_i \bar{A}_i$ , is a three-dimensional quantity in  $x, y, t$ . It can be visualized as a movie (see online examples).

We consider frequencies in 1 mHz-wide bands, centered on the values  $\nu_0 = 1, 3, 5$ , and 7 mHz. The temporal Nyquist frequency for the ISOON cadence is 8.3 mHz. The data sets in this study are approximately 420 minutes in length. Since segments from which we compute the amplitude spectrum are only 60 min in length, the frequency sampling is  $d\nu \sim 0.28$  mHz. Therefore, the average over each 1 mHz band uses about 3-4 images. We have done experiments with shorter and longer  $T$ , as well as with different bandwidths and central frequencies, and the results are qualitatively similar to those shown in § 4.

## 4. Results

We compute and study FFAMs of the oscillatory dynamics associated with the ISOON flaring events at different frequencies, and discuss the active region oscillations and the filament oscillations separately.

#### 4.1. Oscillations in flare regions

The active regions in which the flares occur in the 2005 and 2006 events show oscillatory features over the entire frequency range studied here. The likelihood of a strong contribution from the underlying photospheric acoustic  $p$  modes can be ruled out for several reasons. The dramatic increase in amplitude occurs only once the flare erupts. If the  $p$  modes were responsible, their effects would be present over the entire data sequence. Secondly, the frequency range considered here is mostly below the photospheric acoustic-cutoff frequency ( $\sim 5.3$  mHz). The filter bandpass of ISOON is also quite narrow, much more so than the instrument used by Harvey et al. (1993), where both 5- and 3-minutes oscillations were seen in  $H\alpha$ . We are confident that the effects studied here are confined mostly to the chromosphere.

Figure 2 shows oscillations as a function of frequency in one snapshot of the FFAM from velocity data for flare regions  $FR_1$  and  $FR_2$ . The central time of the 60-min segment used in the computation is provided. The figures represent the slice at the maximal amplitude of the time series. For  $FR_1$ , the UT 16:22 moment is about 9 minutes after the flare erupted. Thus, there is both pre- and post-flare signal in the derived amplitude. For  $FR_2$ , the 18:17 slice is about 23 minutes before the flare erupted, thus there is mostly pre-flare signal involved in the computation.

It is evident from the figure that the flares “excite” all frequencies from about 0.5 to 7.5 mHz to detectable amplitudes in velocity (note the figure is on a logarithmic scale). We are unaware of any previous studies that demonstrate this. The velocities in the 1 mHz band reach about  $3 \text{ km s}^{-1}$  and  $4 \text{ km s}^{-1}$  at peak amplitude for 2005 and 2006 data, respectively, and are usually reduced at higher frequencies. The stronger amplitudes in  $FR_2$  could be due to the fact that it is near the limb, thus implying stronger horizontal motions. Interestingly, the 2006 flare’s maximal amplitude is in the 3 mHz band, at about  $5 \text{ km s}^{-1}$ . In intensity the higher frequencies near each flare contribute much less oscillatory power, as is discussed further in Sec. 4.3.

Once the flare erupts, the excess oscillatory amplitude lasts for about 100 minutes after the peak in the FFAM, although this strongly depends on the location near the ribbons. Some regions are damped much faster or more strongly than others. Due to the 60 min time-averaging involved in creating the FFAMs, it is not convenient to determine the precise duration of the increase in oscillation amplitude, as the time resolution is insufficient to give certainty to this number. More spatial structure is seen in the 1 mHz band, especially in the plage area of the active regions, and the two flare ribbons in  $FR_1$  are somewhat visible in the oscillation amplitudes, as is the sunspot on the northern edge. FFAMs were computed using the ISOON  $H\alpha$  line core (intensity) data as well, and the same general spatial characteristics

are seen, except for weaker power at high frequencies.

## 4.2. Low-frequency oscillations in filaments

Throughout these two data sets the solar disk was littered with quiescent filaments. We identify and analyze two of them for each event, denoted by  $FL_{1-4}$ . The FFAMs show a very dramatic “lighting up” (a rapid increase in oscillation amplitude) of the filaments well after the distant flares erupt, although each event has somewhat different characteristics.

Figure 3 shows snapshots from the FFAM of filaments  $FL_1$  and  $FL_2$  in the 2005 time series. The images are those where the filament oscillation amplitude peaks in the FFAM, corresponding to the time segment centered at 55 and 62 minutes after the flare erupts for  $FL_1$  and  $FL_2$ , respectively. One explanation of the different timings is that the filaments are at different distances from the flare center (see Fig. 1), and whatever activation mechanism is at work (such as a chromospheric wave) needed to travel different distances.

The noticeable difference compared to the oscillations in the flare region, is that the filament only shows strong amplitude excess in the lowest frequency bandpass of  $1 \pm 0.5$  mHz, even on the logarithmic scale. This corresponds to periods in the range from about 11 to 33 minutes. The amplitude is significantly above the background level in this passband, lasting for about 100 minutes. The velocities of the oscillations are on the order of  $0.5 - 1.0 \text{ km s}^{-1}$ . This is the first detection of oscillatory behavior in these two particular filaments.

As in previous studies (Tripathi et al. 2009), one might conclude that anywhere from about 3 to 10 periods of the filament oscillation took place after it was excited. With our method, it may be too simplistic to make such a conclusion, since there are small-scale spatial structures that are operating on different time scales, as is clearly evident in the FFAMs. Some regions show low-frequency power for the whole duration (like the central part of the filament), while others do not (the “ends” of the filament).

The 2006 quiescent filaments are shown in Fig. 4. We note again that a strong Moreton wave was associated with this flare that propagated outwardly from the active region at speeds up to  $1600 \text{ km s}^{-1}$  (Balasubramaniam et al. 2010). The wave passed near both filaments and presumably activated their oscillations. The maximum values of the amplitudes in this case are  $\approx 0.2 \text{ km s}^{-1}$ , less than half the strength than found in the  $FL_1$  and  $FL_2$  filaments. Filament  $FL_3$  shows no oscillations in its center, only on its ends, which is a curious feature. Additionally, even though these two filaments are not equidistant to the flare region, the maximal oscillation amplitude occurred at approximately the same time.



That the velocity oscillation signal in the filaments is weaker than in the 2005 event is surprising, given that there is a clear and strong Moreton wave observed that interacts with the filaments. Possible explanations for this discrepancy might include viewing geometry, intrinsic difference in filament properties, lower quality of data, or the overall distance of the filaments from the flare, which is larger than in the 2005 case.

### 4.3. Comparison of method to other analysis techniques

Analyzing one-dimensional time series of various regions by wavelet analysis is one technique that has become standard for the study of filament oscillations (e.g., Pintér et al. 2008). Computing “stack plots” of the signal along a certain slice of the data as a function of time is another (e.g., Li & Zhang 2012). We carry out such analyses to compare and contrast the results with those of the FFAMs for the flare  $FR_1$  and filament  $FL_1$  regions. The other regions show similar behavior.

Figure 5 shows an analysis of  $FR_1$ . A set of pixels near the flare ribbons was averaged and time series of intensity and velocity were obtained. The intensity light curve shows the characteristic flare impulse and exponential decay, accompanied by low-level oscillations, while the velocity shows a fluctuating signal on top of a sudden blueshift (towards observer) as the flare erupts. Other pixels in the flare-ribbon region show redshifts at flare onset (for a detailed discussion of velocity profiles in broadband  $H\alpha$  measurements, see Ichimoto & Kurokawa 1984). In both cases the frequency content of the oscillations are difficult to quantify in the time series alone. Wavelet analysis of this set of pixels confirms that all frequencies in velocity are activated, but that the low frequencies are strongest, as the FFAMs indicated. The strongest amplitudes last for about 80 minutes. The spectrum in intensity does not show much high-frequency power. These conclusions change somewhat as different regions are analyzed.

Perpendicular slices through the flare ribbons passing through the center of the same set of pixels are used to produce stack plots for intensity and velocity and are given in Fig. 6. From the horizontal slice one sees that the east side of the flare (closest to point C) is the first to begin oscillating, as is evident also in the FFAM. The strongest signal comes from the outer edge of the ribbons. The velocity stack plots indicate that the east-west direction (C-D) has a higher signal-to-noise, even though the other direction has the larger overall amplitude.

Figure 7 shows a similar analysis for the filament  $FL_1$ . A set of pixels near the center of the filament that showed strong oscillations in velocity were chosen and averaged to give



the time series. There are 6-7 long-period oscillations ( $\sim 20$  min) at amplitudes of about  $1 \text{ km s}^{-1}$  in this region, and these show up clearly in the wavelet spectra. In intensity, the variations in the time series are less well defined, but the wavelet spectra do reveal the low-frequency nature of the oscillations. Contrasting with the chosen flaring region, the strong amplitudes near the filament persist for well over 100 minutes. The stack plots in Fig. 8 show slices through the filament along perpendicular directions. Again, the global view of the intensity slice is not particularly useful for studying any variations, while the velocity plots clearly show the filament being triggered by the flare and its subsequent oscillations. The motion appears to be primarily in the east-west longitudinal direction.

The use of these standard techniques are indeed very useful for studying these phenomena, especially when coupled with an analysis using FFAMs. However, the choice of pixels and slice coordinates to produce Figs. 5-8 requires a lot of trial and error, and the inferences vary strongly from region to region. This could be expedited by first using the FFAMs to choose suitable regions that show interesting behavior, and then looking into more detail with the other methods. It is interesting that the stack plots in intensity for the filament do not strongly show the flare eruption, at least along these particular slices, while the intensity FFAMs and wavelets clearly do.

#### 4.4. Summary of results

To summarize the analyses, we observe the fascinating occurrence of rapid communication at large distances across the solar disk. In the 2005 event, strong amplitude increases on the far western solar limb are observed, very far from the flare area in the eastern hemisphere. Indeed, Fig. 9 shows full-disk snapshots of velocity FFAMs in the two lowest bandpasses near the peak flaring times. The filamentary amplitudes are evident everywhere at low frequency, and rather absent at 3 mHz and higher. For the 2006 flare, the 1 mHz band shows weak excess acoustic power just outside the flare region, and one barely discerns the brightenings in filaments FL<sub>3</sub> and FL<sub>4</sub> in this global picture.

A comparison with other large-amplitude filament oscillations as reviewed by Tripathi et al. (2009) and Arregui et al. (2012) is useful. Other published studies find oscillations with minimum amplitudes near  $20 \text{ km s}^{-1}$ . Gilbert et al. (2008) find in line-of-sight velocity images from the Polarimeter for Inner Coronal Studies (PICS) H $\alpha$  instrument that the FL<sub>3</sub> filament oscillates at amplitudes up to  $41 \text{ km s}^{-1}$ . We find amplitudes of a few  $\text{km s}^{-1}$  in the flare regions themselves, but less than  $1 \text{ km s}^{-1}$  in the filaments at low frequency. In the raw Doppler signal from ISOON we find maximum velocities of the FL<sub>3</sub> filament of several  $\text{km s}^{-1}$ .

While we do observe features that approach several tens of  $\text{km s}^{-1}$  in the line-of-sight velocity data, particularly in the flare (see Fig. 6, for example), the coherent variations over an extended time period do not possess such amplitudes. We attribute the discrepancy with other values in the literature to the fact that the FFAMs select out the persistent variations over longer time scales (in the computations here, at least 60 min), and thus it is a matter of effective time resolution. Differences in instrumentation likely have some effects too.

For filament oscillation periods, studies have found a range from about 6 to 150 minutes (Tripathi et al. 2009). The periods found here are on the lower end of those values, but still consistent with them. One might argue that small-amplitude oscillations are a suitable classification for these events, which tend to have a few  $\text{km s}^{-1}$  amplitudes, but can also have very short periods on the order of seconds to a few minutes, which we are unable to observe.

Gilbert et al. (2008) have already studied both  $\text{FL}_3$  and  $\text{FL}_4$  using different data and standard methods. For  $\text{FL}_3$ , they find 3 hr of oscillatory motions, somewhat longer than found here by about 30 minutes. They also find periods from 18-39 min. For  $\text{FL}_4$  they find the duration of oscillations to be only about 17 minutes, whereas we observe increased power (at 1 mHz) for more than 1 hr. The different diagnostics as a function of frequency is an advantage of the method presented here.

## 5. Discussion

This work is important for two reasons: (1) we have presented a simple algorithm for both visualizing and studying dynamic phenomena in 2+1 dimensions with differing frequency content; (2) we have used this technique to analyze two different events that exhibit low-frequency filament oscillations excited by a distant flare. We observe robust oscillations in the active regions where the flares erupt over a broad range of frequencies. Photospheric modes can be ruled out as the source since the oscillation amplitude only increases after the flare initiates.

Strangely, the weaker filament oscillations are observed in the system that interacted with a strong Moreton wave, which can trigger of such oscillations, but it is possible that line-of-sight effects or wave propagation direction can be involved in these differences. The velocities found in the FFAM analysis do not fit into the large- and small-amplitude oscillation classifications. It might be useful to have sub-categories of such events that show oscillating strengths as a function of frequency. We have been able to confirm the work of Gilbert et al. (2008) who showed that the  $\text{FR}_4$  filament is a lower-amplitude oscillator than the other filament in the December 2006 flare event.

The spatial features of the velocity power in the different frequency bands show interesting dynamics, particularly for the filaments. We observe different sections of the filaments fluctuating over various timescales, indicating that either the damping of the oscillations is spatial dependent or the excitation is not constant over the entire length of the filaments, or some combination of both effects. More detailed analysis of this is underway.

There is both new and complementary information when comparing the original full-disk time series and the FFAMs (the movies associated with Fig. 1 and the FFAMs of Fig. 9). For example, for the 2005 event, in the raw intensity time series one clearly sees the reaction of some of the far-away filaments after flare eruption, but the FFAM indicates that some filaments are actually not affected by the (unknown) trigger mechanism, and also directly provides the oscillation frequencies of those which are. In the 2006 flare the Moreton wave is easily visible in both intensity and Doppler data, yet the response of the filaments is rather muted when viewed in the FFAM, suggesting that the oscillation activation was not as effective. Certainly more events need to be treated in such a systematic fashion to understand if these are common occurrences or not.

We finally point out that at the photosphere, active regions typically show an enhancement of acoustic power at *higher* frequencies, known as acoustic halos (Braun et al. 1992). This is quite different than the case here where we see higher amplitudes in the lower-frequency bandpasses. How the frequency content of waves changes through the different layers of the atmosphere could help in understanding the local environment parameters that are quite difficult to directly observe, such as magnetic field and density. EUV waves can also presumably interact with filaments, although for the two events studied here there were no EUV data that could be used to identify any such contribution. In the future this method will be used to study a range of various chromospheric data.

We acknowledge fruitful conversations with Stuart Jefferies, Michael Kirk, Frank Hill, and R.T. James McAteer. This work was supported in part by an NSF PAARE award AST-0849986.

## REFERENCES

- Arregui, I., Oliver, R., & Ballester, J. L. 2012, Living Reviews in Solar Physics, 9, 2
- Asai, A., Ishii, T. T., Isobe, H., et al. 2012, ApJ, 745, L18
- Balasubramaniam, K. S., Christopoulou, E. B., & Uitenbroek, H. 2004, ApJ, 606, 1233

- Balasubramaniam, K. S., Pevtsov, A. A., & Neidig, D. F. 2007, *ApJ*, 658, 1372
- Balasubramaniam, K. S., Cliver, E. W., Pevtsov, A., et al. 2010, *ApJ*, 723, 587
- Bisi, M. M., Breen, A. R., Jackson, B. V., et al. 2010, *Sol. Phys.*, 265, 49
- Braun, D. C., Lindsey, C., Fan, Y., & Jefferies, S. M. 1992, *ApJ*, 392, 739
- Elliott, I. 1969, *Sol. Phys.*, 6, 28
- Eto, S., Isobe, H., Narukage, N., et al. 2002, *PASJ*, 54, 481
- Gilbert, H. R., Daou, A. G., Young, D., Tripathi, D., & Alexander, D. 2008, *ApJ*, 685, 629
- Harvey, J. W., Duvall, Jr., T. L., Jefferies, S. M., & Pomerantz, M. A. 1993, in *Astronomical Society of the Pacific Conference Series*, Vol. 42, *GONG 1992. Seismic Investigation of the Sun and Stars*, ed. T. M. Brown, 111–+
- Ichimoto, K., & Kurokawa, H. 1984, *Sol. Phys.*, 93, 105
- Isobe, H., & Tripathi, D. 2006, *A&A*, 449, L17
- Jain, R., & Tripathy, S. C. 1998, *Sol. Phys.*, 181, 113
- Kazachenko, M. D., Canfield, R. C., Longcope, D. W., et al. 2009, *ApJ*, 704, 1146
- Li, T., & Zhang, J. 2012, *ApJ*, 760, L10
- Liu, C., Lee, J., Yurchyshyn, V., et al. 2007, *ApJ*, 669, 1372
- Maurya, R. A., & Ambastha, A. 2008, *Journal of Astrophysics and Astronomy*, 29, 249
- Neidig, D., Wiborg, P., Confer, M., et al. 1998, in *Astronomical Society of the Pacific Conference Series*, Vol. 140, *Synoptic Solar Physics*, ed. K. S. Balasubramaniam, J. Harvey, & D. Rabin, 519
- Okamoto, T. J., Nakai, H., Keiyama, A., et al. 2004, *ApJ*, 608, 1124
- Pintér, B., Jain, R., Tripathi, D., & Isobe, H. 2008, *ApJ*, 680, 1560
- Ramsey, H. E., & Smith, S. F. 1966, *AJ*, 71, 197
- Tripathi, D., Isobe, H., & Jain, R. 2009, *Space Sci. Rev.*, 149, 283
- Vršnak, B., Veronig, A. M., Thalmann, J. K., & Žic, T. 2007, *A&A*, 471, 295

Yurchyshyn, V., Liu, C., Abramenko, V., & Krall, J. 2006, Sol. Phys., 239, 317

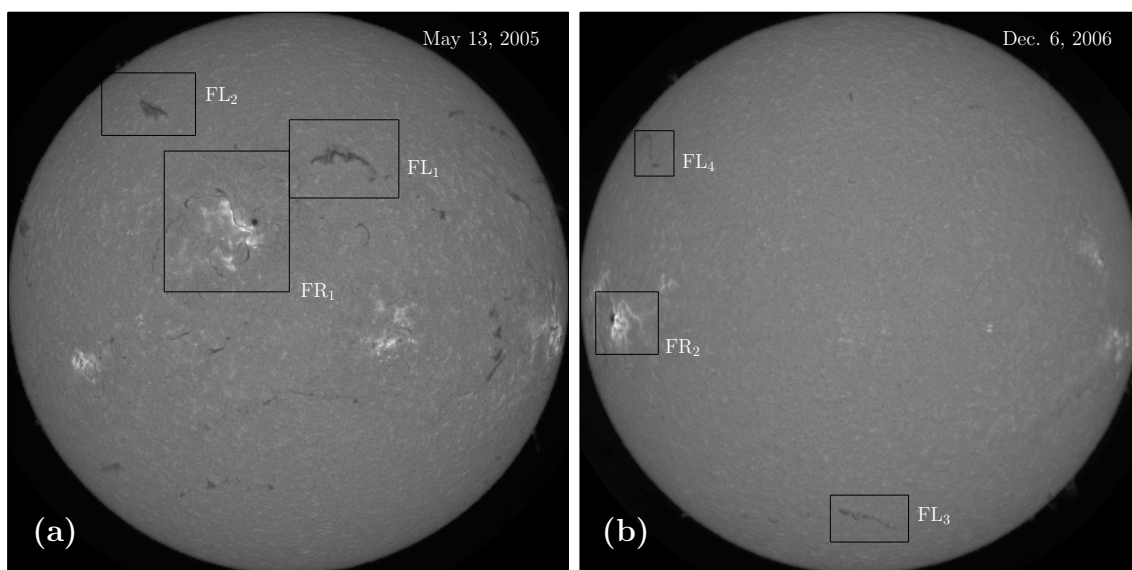


Fig. 1.— Snapshots (pre-flare) in  $H\alpha$  intensity from the ISOON telescope for the (a) 2005 M-class flare and the (b) 2006 X-class flare. Three regions of interest are marked for each event, where “FR” denotes a flaring region and “FL” denotes a filament. See online version for movies of the intensity and Doppler time series. You can view all movies online at [http://astronomy.nmsu.edu/jasonj/Halpha\\_movies/](http://astronomy.nmsu.edu/jasonj/Halpha_movies/).

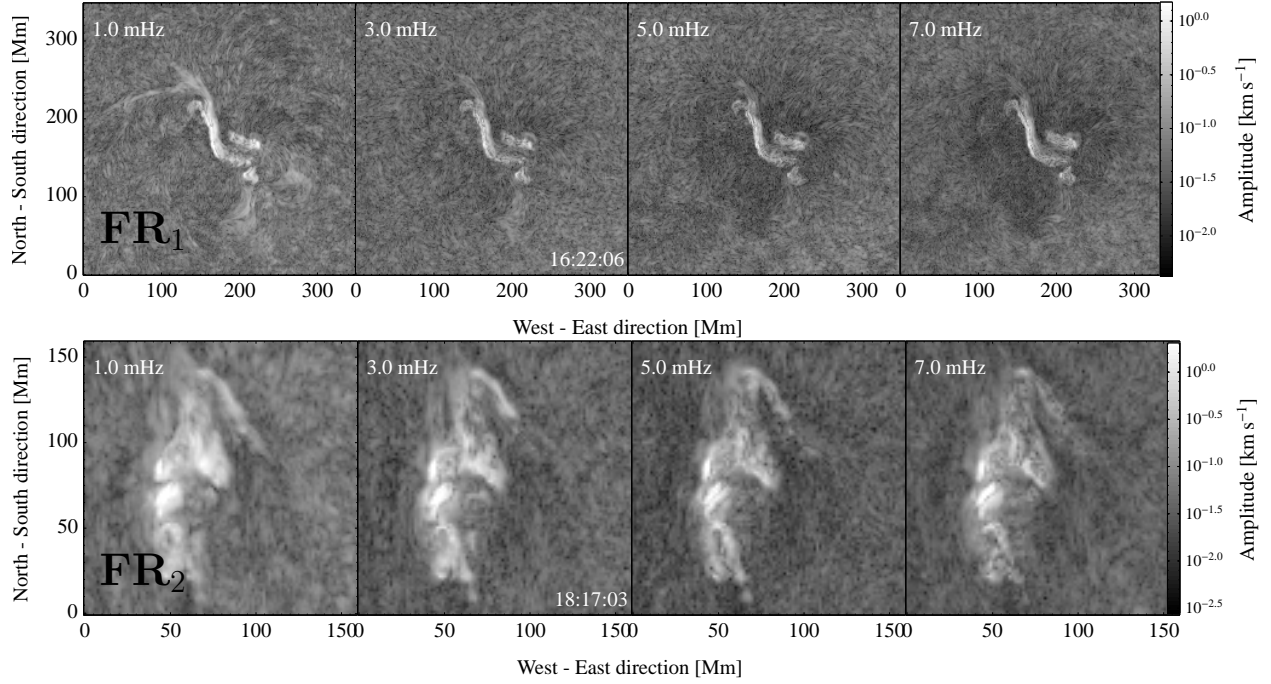


Fig. 2.— The two flaring regions. Each panel is a snapshot of an FFAM, showing the logarithm of the amplitude computed from 60 min of H $\alpha$  velocity data for the 1, 3, 5, and 7 mHz frequency bands, from left to right. The top (bottom) row shows the amplitude in the flare region FR<sub>1</sub> (FR<sub>2</sub>) from segments centered at about 9 and 23 minutes after flare initiation, respectively. The color scale is clipped at 0.5 of the maximum velocity amplitude to emphasize smaller scale features. See online version for full FFAMs of both intensity and velocity for each frequency and flare event.



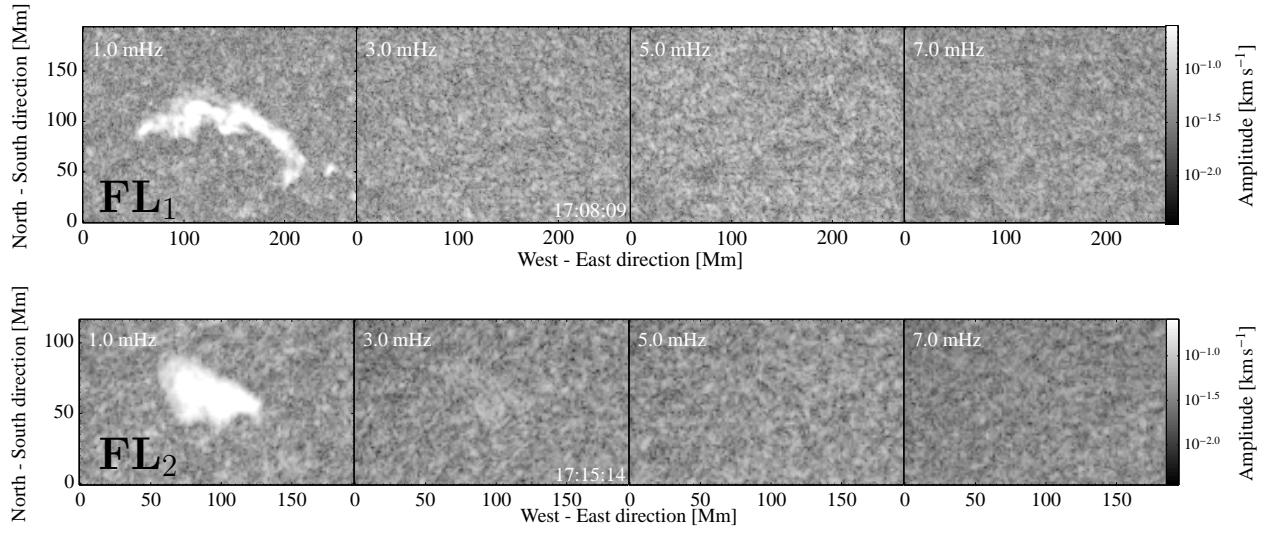


Fig. 3.— Filaments during the May 13, 2005 flare. Each panel is a snapshot of an FFAM, showing the logarithm of the amplitude computed from 60 min of H $\alpha$  velocity data for the 1, 3, 5, and 7 mHz frequency bands, from left to right. The top (bottom) row shows the amplitude in two quiescent filament regions FL<sub>1</sub> (FL<sub>2</sub>) for each frequency passband, about 55 and 62 minutes after flare eruption, respectively. The color scale is clipped at 0.5 of the maximum velocity amplitude. See online version for full FFAMs.

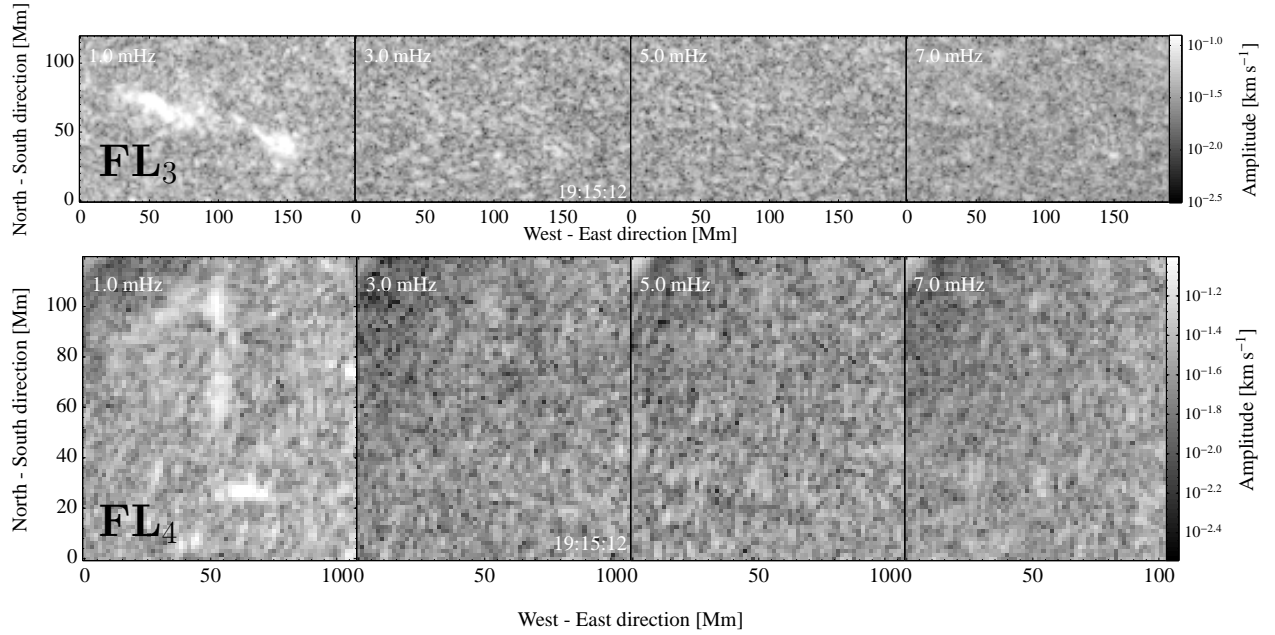


Fig. 4.— Filaments during the December 6, 2006 flare. Each panel is a snapshot of an FFAM, showing the logarithm of the amplitude computed from 60 min of H $\alpha$  velocity data for the 1, 3, 5, and 7 mHz frequency bands, from left to right. The top (bottom) row shows the amplitude in two quiescent filament regions FL<sub>3</sub> (FL<sub>4</sub>) for each frequency passband, about 35 minutes after flare eruption. The color scale is clipped at 0.5 of the maximum velocity amplitude. See online version for full FFAMs.

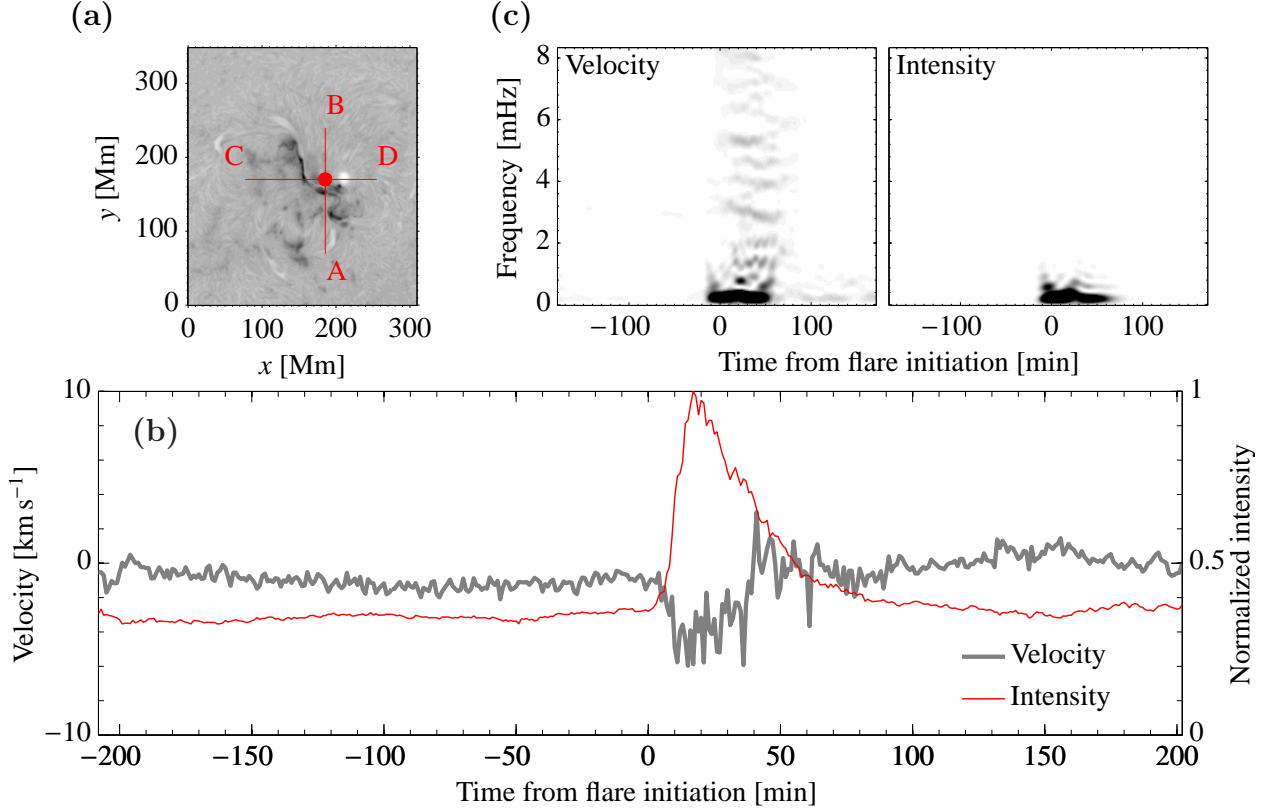


Fig. 5.— Analysis of flare FR<sub>1</sub> using standard methods. (a) A snapshot of intensity around the flare. The red circle indicates the pixels (radius of 10 pixels) that were averaged to compute the time series in panel (b). The horizontal and vertical lines denote slices used for the plots in Fig. 6. (b) Time series of normalized intensity and Doppler velocity for the set of pixels in the flare region as a function of time. (c) Wavelet power spectra of the velocity and intensity light curves from (b). The (linear) gray scale in these plots is such that black denotes higher signal, and has been clipped to half of the maximum power to emphasize details.

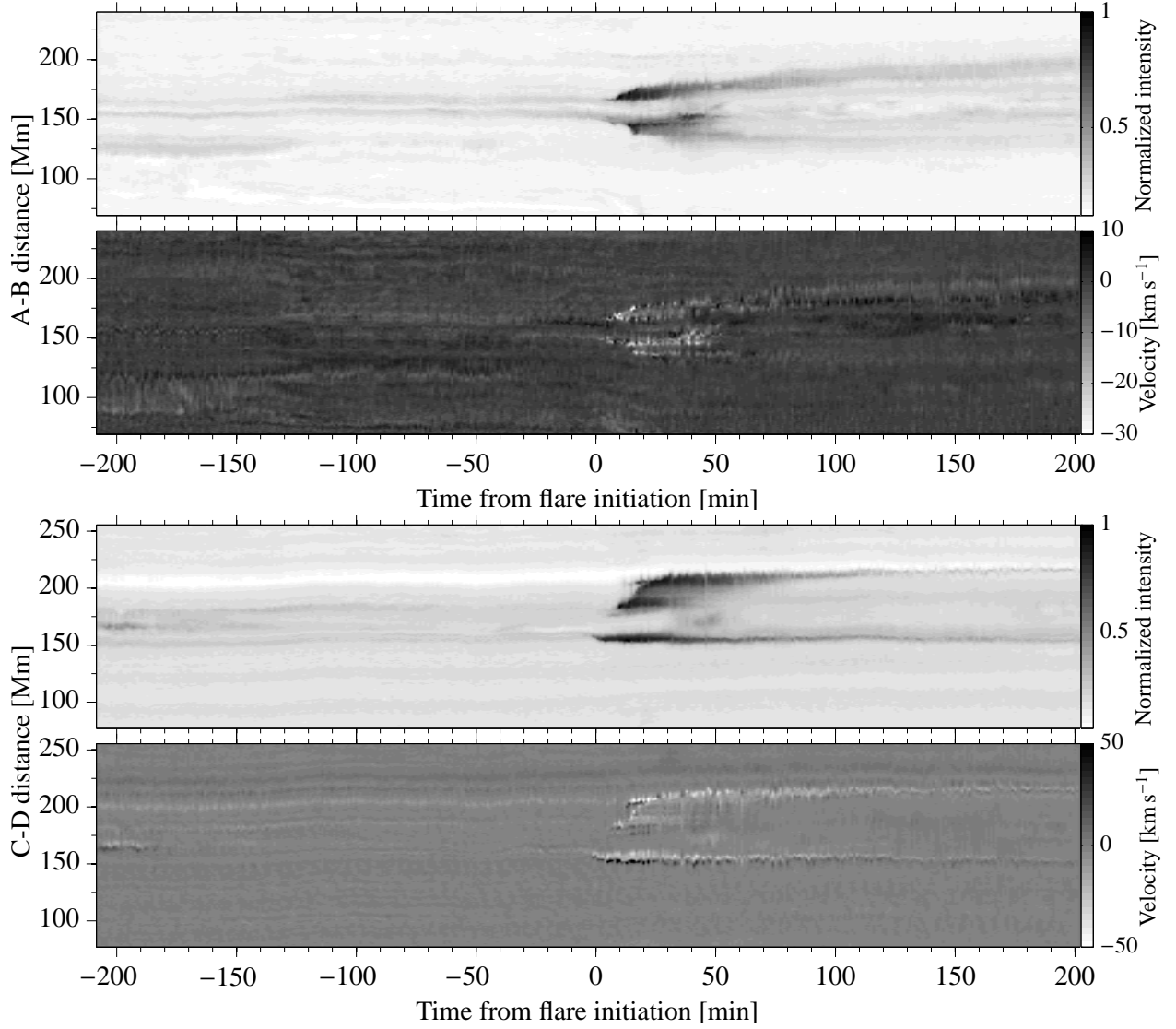


Fig. 6.— Stack plots of flare FR<sub>1</sub> along the slices indicated in Fig. 5a. The top two panels show the intensity and velocity time dependence along the A-B vertical line through the flare. The bottom two panels show the intensity and velocity time dependence along the C-D horizontal line through the flare.

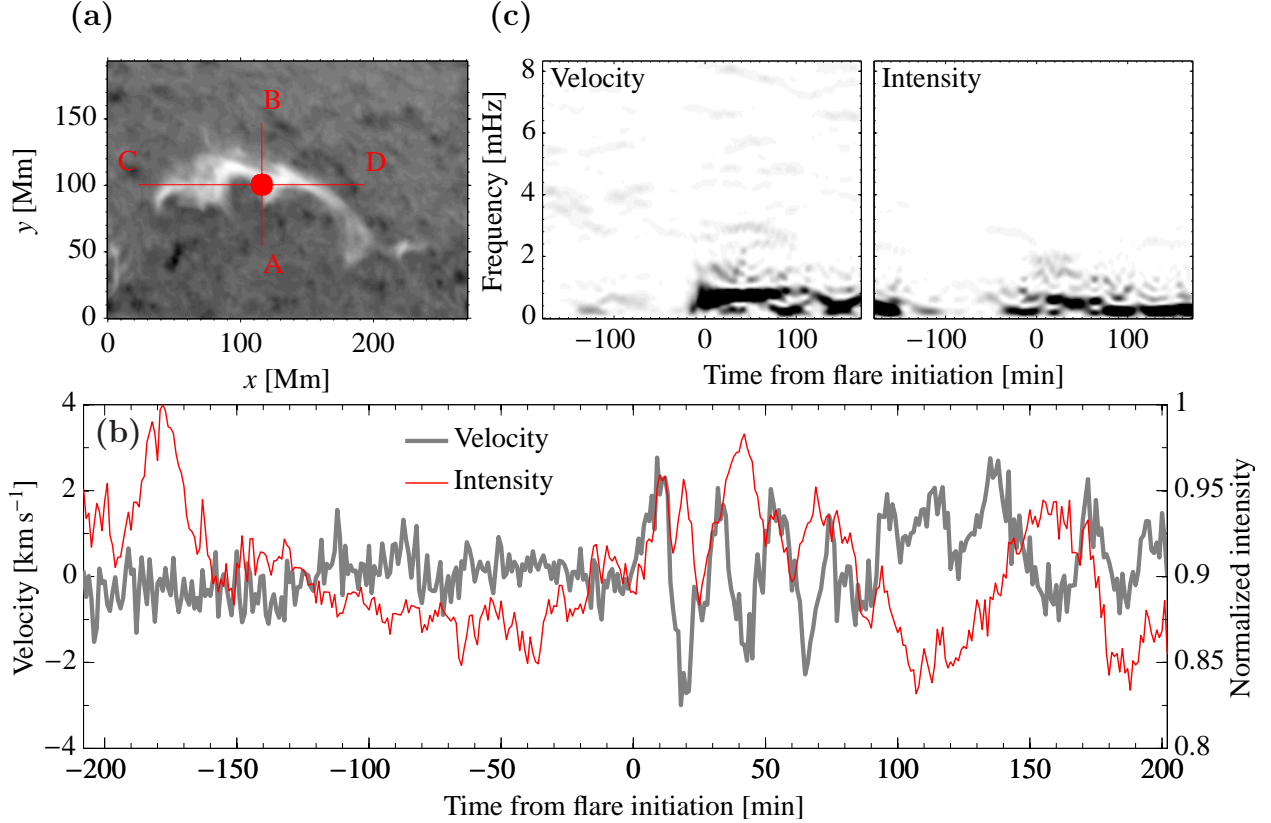


Fig. 7.— Analysis of filament FL<sub>1</sub> using standard methods. (a) A snapshot of intensity around the filament. The red circle indicates the pixels (radius of 10 pixels) that were averaged to compute the time series in panel (b). The horizontal and vertical lines denote slices used for the plots in Fig. 8. (b) Time series of normalized intensity and Doppler velocity for the set of pixels in the filament region as a function of time. (c) Wavelet power spectra of the velocity and intensity light curves from (b). The (linear) gray scale in these plots is such that black denotes higher signal, and has been clipped to half of the maximum power to emphasize details.

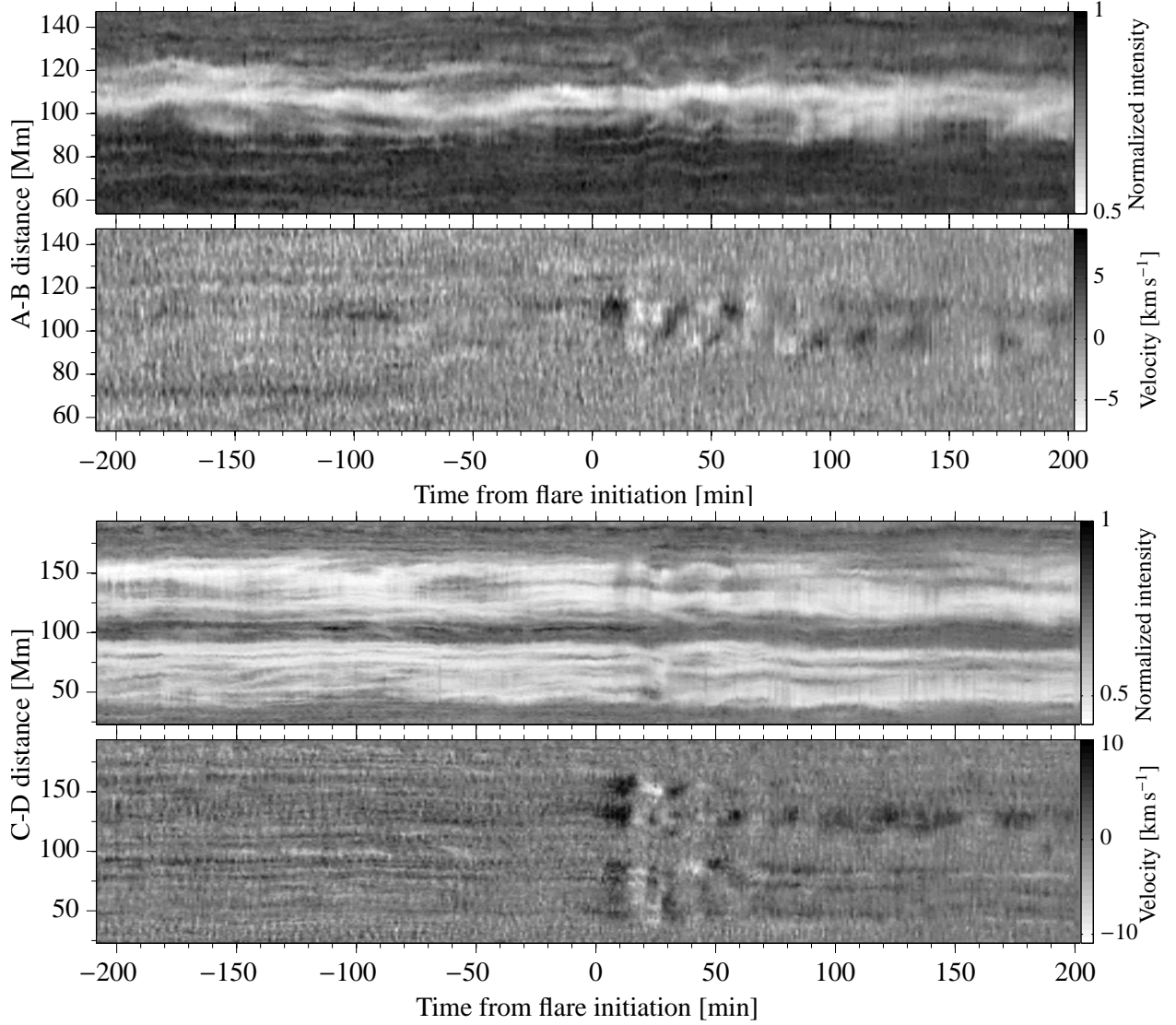


Fig. 8.— Stack plots of filament FL<sub>1</sub> along the slices indicated in Fig. 7a. The top two panels show the intensity and velocity time dependence along the A-B vertical line through the filament. The bottom two panels show the intensity and velocity time dependence along the C-D horizontal line through the filament.



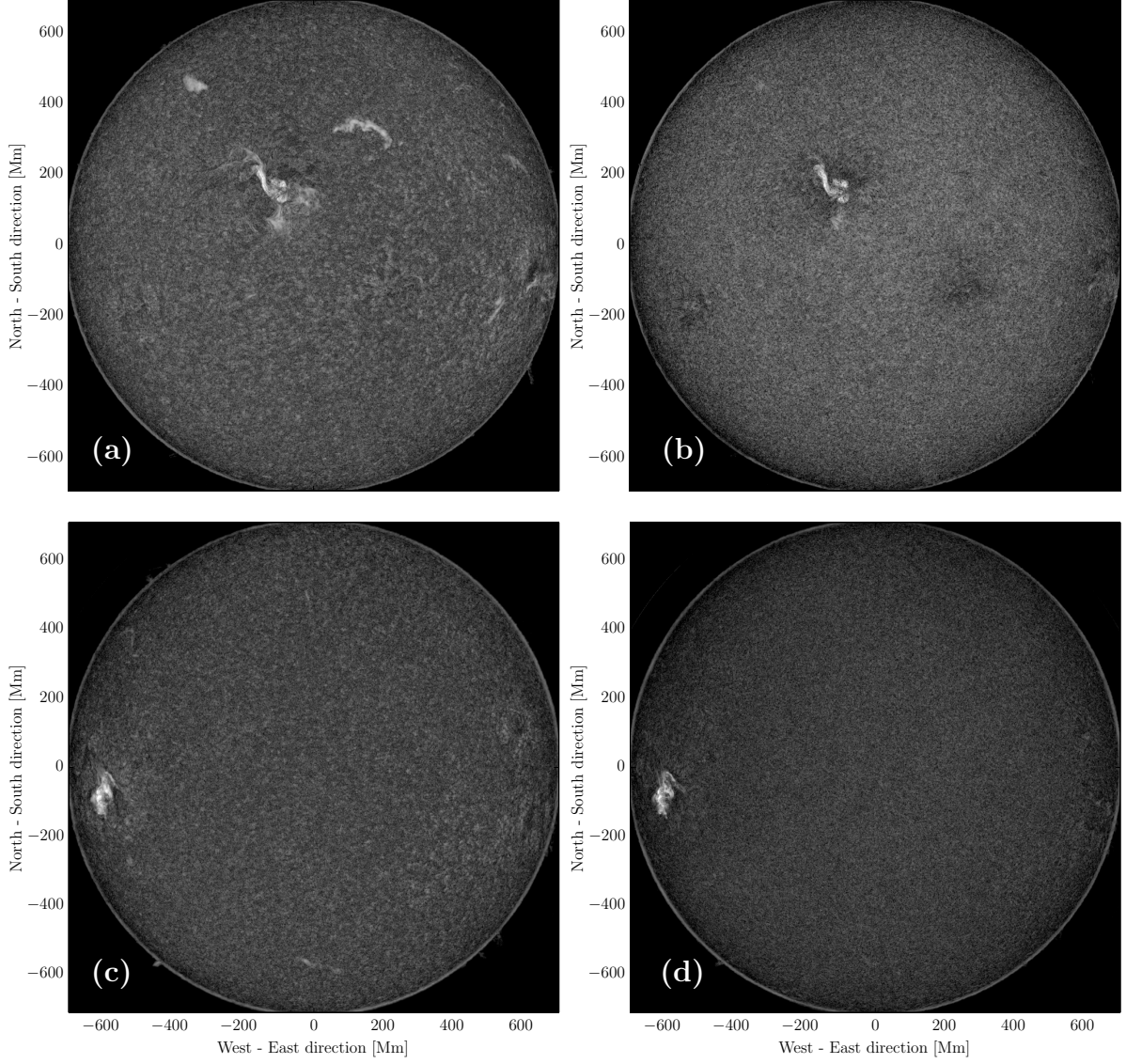


Fig. 9.— Snapshots of full-disk velocity FFAMs around peak flare intensity. Panels (a) and (b) are the 1 mHz and 3 mHz bands for the 2005 flare, respectively. Panels (c) and (d) are the 1 mHz and 3 mHz bands for the 2006 flare, respectively. All panels are plotted on the same gray scale. See the full-disk FFAMs online.